Numerical analysis of oil combustion in a small combustion device

Numerična analiza oljnega gorilnika v mali kurilni napravi

Matej Zadravec[1,*], Boštjan Rajh[2], Niko Samec[1], Matjaž Hriberšek[1]

[1] Faculty of Mechanical Engineering, University of Maribor, Smetanova 17, 2000 Maribor, Slovenia
[2] EnerB d.o.o., Hmeljarska ulica 7, 3310 Žalec, Slovenia

E-Mails: matej.zadravec@um.si ; bostjan.rajh@enerbee.eu ; niko.samec@um.si ; matjaz.hribersek@um.si

* Corresponding author

Abstract: This paper focuses on the numerical analysis of the combustion of the liquid fuel Extra Light Fuel Oil (ELFO) in a small combustion device. The calculation was performed by ANSYS CFX computer code for experimental optimal air-fuel ratio (λ_{opt}) and the middle power of the oil burner Weishaupt WL5/1-A (37 kW). The goal of the numerical analysis was to establish, whether the experimentally determined λopt ensured the conditions for a complete combustion in each point of the combustion chamber. The comparison of numerical results and measured values confirm the suitability of the chosen numerical model.

Key words: oil burner, oil combustion, multicomponent reactive flow, computational fluid dynamics (CFD), model validation.

Povzetek: Prispevek obravnava numerično analizo zgorevanja v oljnem gorilniku ekstra lahkega kurilnega olja (ELKO) v mali kurilni napravi. Numerična analiza je bila izvedena v programskem paketu ANSYS CFX pri eksperimentalno določenem optimalnem razmerju zraka in olja (λ_{opt}) in srednji moči oljnega gorilnika Weishaupt WL5/1-A (37 kW). Namen numerične analize je bil preveriti ali eksperimentalno določeno optimalno razmerje (λ_{opt}) zagotavlja popolno zgorevanje v vsakem območju kotla male kurilne naprave. Ujemanje med eksperimentalnimi podatki in izbranimi parametri za numerično analizo kažejo dobro ujemanje.

Ključne besede: oljni gorilnik, zgorevanje olja, večkomponentni reaktivni tok, računalniška dinamika fluidov (RDF), validacija modela.

1. Introduction

A detailed analysis of the combustion process under actual operating conditions of a specific combustion device requires considering of all diffusion and reaction processes of reacting flow at the same time. Next to the chemical kinetics, the impact of convection, diffusion and other physical processes have to be taken into account. Monitoring of all stated processes during the experiment is very difficult or even impossible. Therefore, Computational Fluid Dynamics (CFD) is being increasingly used in industry for the purposes of consideration and more detailed analysis of combustion processes as well as for optimization of combustion devices. The greatest issue in modeling the turbulent reacting flow is the fact that the majority of numerical models are based on empirical presuppositions. Therefore, an experiment has to be carried out in order to determine the missing parameters that are necessary for an appropriate numerical model.

In the field of ELFO combustion, only a few literature sources [1] focusing on determination of wall heat fluxes in the large scale test combustors can be found. Some other sources [2] focus on the combustion of light residual fuel oils. Many authors have been studied CFD modeling of heavy fuel oil combustion [3-5]. In general it is not possible to find any sources dealing with the CFD numerical model as a whole used for ELFO combustion in a small combustion device to analyse the achievement of complete combustion conditions in the whole space of combustion chamber.

2. Combustion in a small combustion device

Oil burners are appliances that heat the home using fuel oil. Oil is delivered to the home and pumped into a storage tank. Oil from the storage tank is drawn into the oil burner. The oil burner atomizes the oil (turns it into a mist of tiny oil droplets), mixes it with air and ignites it with a spark. The resulting flame shoots out of the blast tube and into the oil burner chamber (see fig. 1). Combustion gasses move through the heat exchanger where heat is transferred to the household air stream. The combustion gasses then make their way up the flue and out of the house.

All practical combustion processes are turbulent in nature. Turbulent non-premixed flames are encountered in a large number of industrial systems for two main reasons. The first, compared to premixed flames, non-premixed burners are simpler to design and to build because a perfect reactant mixing, in given proportions, is not required. Moreover, non-premixed flames are also safer to operate as they do not exhibit propagation speeds and cannot auto-ignite in undesired locations [6].

On the basis of experimental measurements of flue gas emissions, carried out by a flue gas analyzer for different air-fuel ratios (λ=1.15, λ=1.2 and λ=1.3), the optimal air-fuel ratio λopt = 1.2 was determined. It enables well operation of a combustion device under different conditions (permanent changes of air pressure, of air temperature and of pressure in the furnace as well as other weighting factors) within one service interval. In the scope of the experiment, specific data necessary for creation of the numerical model were obtained. This was performed by determining the λopt representing most optimal operating conditions, by creating the precise geometry of the furnace and the oil burner, and by collecting data concerning the oil nozzle. After that, we attempted to define an appropriate numerical model by applying the CFD. This model makes it possible to examine, whether the appropriate λopt was determined during the experiment, and if conditions for complete combustion are provided in every point of combustion chamber.

(a)   (b)
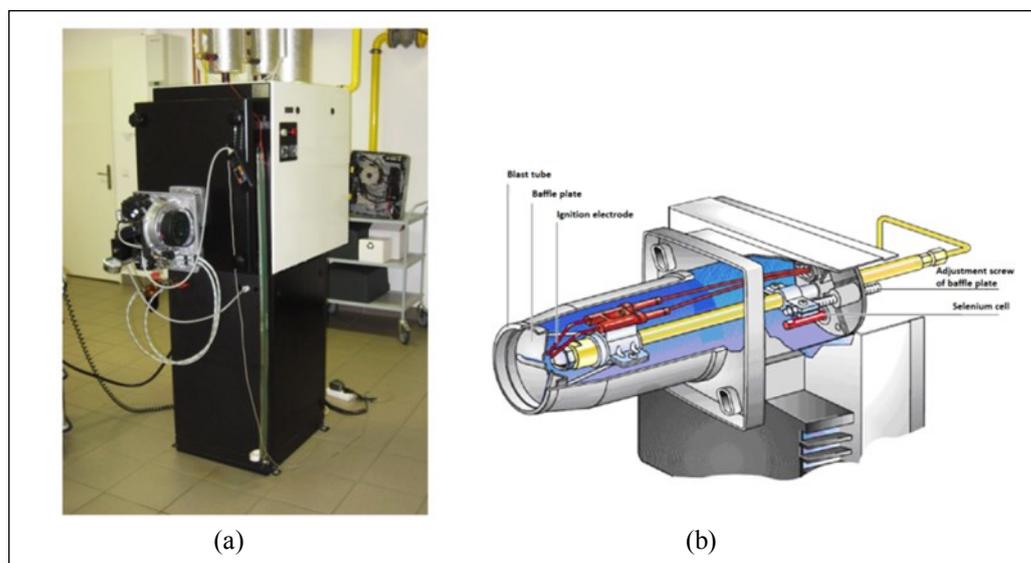
Figure 1. (a) Experimental furnace Weishaupt. **(b)** Mixing device of the oil burner Weishaupt WL5/1-A.

Liquid ELFO evaporation and combustion process are described by a numerous of evaporation and combustion models which are available to address many different applications. These applications are characterized by the type of mixing (e.g. non-premixed, premixed or partially premixed) and reaction chemistry (e.g. finite-rate chemistry or fast chemistry). The applied model contains the liquid Jet-A fuel $C_{12}H_{23}$ (average composition of ELFO) as a pure substance with specified adequate substance properties ($\rho = 840$ kg/m^3, $\eta = 0.00336$ kg/ms, $\lambda = 0.14$ W/mK, latent heat = 280 kJ/kg at 70 °C, surface tension coefficient of oil = 0.026 N/m). The Liquid Jet-A Fuel $C_{12}H_{23}$ evaporates into its equivalent gas phase.

Combustion primarily takes place in a diffusion-limited mode (non-premixed) where fuel and oxidant are brought into contact via mixing and can then react. In these flames, it can generally be assumed that the turbulent mixing rate is much slower than the chemical kinetics rates (fast chemistry), and hence, will be the rate-limiting step. The current study uses the Eddy-Dissipation Combustion (EDC) model which assumes that the reaction rate is controlled by the turbulent mixing rate. Hence, the turbulent mixing rate in conjunction with a global reaction mechanism is used to predict local temperatures and species profiles. This model solves the conservation equations describing convection, diffusion, and reaction sources for each component species. The gas phase is a part of changeable gas mixture that burns using a single-step reaction of the two-step reactions mechanism. At the first stage, the reaction specifies the gas phase and O_2 as reactants, while CO and H_2O are determined as combustion products (eq. 1). At the second stage, however, CO and O_2 are specified as reactants, while CO_2 is a combustion product (eq. 2):

$$C_{12}H_{23} + 11.75\,O_2 => 12\,CO + 11.5\,H_2O \tag{1}$$

$$CO + \frac{1}{2}\,O_2 => CO_2 \tag{2}$$
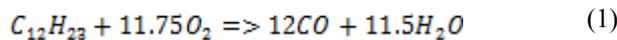
Additionally, the formation of NOX (thermal NO) was included into the model on the basis of Zeldovich mechanism (NO Formation with Temperature PDF).

The selection of suitable reaction rates for chemical reactions is a very difficult task due to a shortage of data as well as ambiguity and inconsistency in scientific resources. After careful review the data of Westbrook and Dryer [7] have been used for $C_{10}H_{22}$ scaled by molar mass. The reaction rates for NO formation were taken from CH_4 combustion mechanism.

3. Numerical model

3.1. Governing Equations

The features of the turbulent flame depend mainly on the nature of the reacting flow. At sufficiently high Reynolds Numbers the flow becomes turbulent. The turbulent flow is unstable; it moves in irregular patterns and contains vortices of different sizes. These eddies move with different rotation and translation motion through the combustion chamber. The contour of the turbulent flow is not steady, but is changing all the time. Also unsteady is the flame front; its boarder surface is extremely curved. Exactly such type of flame is typical of ELFO combustion in a small combustion device. According to many authors [8-9], it is very difficult to establish a precise definition of the turbulent reacting flow. However, it is known that such flow has features like great instability, high value of Reynolds Number, 3D fluctuation of eddies, their dissipation and turbulent diffusion that causes fast mixing of reactants, and increases the relation between momentum and the mass and heat transfer. An adequate description of the movement of incompressible viscous two-phase turbulent reacting flow is given by using the Reynolds-averaged Navier-Stokes (RANS) equations for mass (eq. 3), momentum (eq. 4) and energy (eq. 5) conservation:

$$\frac{\partial \rho}{\partial t} + \frac{\partial}{\partial x_j}\left(\bar{\rho}\bar{v_j}\right) = 0 \tag{3}$$

$$\frac{\partial}{\partial t}\left(\bar{\rho}\bar{v_j}\right) + \frac{\partial}{\partial x_j}\left(\bar{\rho}\bar{v_j}\bar{v_i}\right) = -\frac{\partial p}{\partial x_i} + \overline{f_{vi}} + \frac{\partial}{\partial x_j}\left(\overline{\tau_{ij}} + \overline{\rho v_j' v_i'}\right) \tag{4}$$

$$\frac{\partial}{\partial t}\left(\bar{\rho}\bar{h}\right) + \frac{\partial}{\partial x_j}\left(\bar{\rho}\bar{v_j}\bar{h}\right) - \frac{\partial p}{\partial t} + \frac{\partial}{\partial x_j}\left(q_j + \overline{\rho v_j' h'}\right) = \bar{I}_T + \bar{I}_R \tag{5}$$

$\bar{\rho}$, $\bar{h}$, $\bar{v_j}$ are the mean values of density, enthalpy and fluid velocity, $\overline{f_{vi}}$ is the sum of all volume forces, p is the pressure, $\bar{I}_T$ is the combustion and $\bar{I}_R$ is the radiation source/sink term, $\overline{\tau_{ij}}$ and $\bar{q}_j$ are the viscous stress tensor and the heat flux, respectively.

By applying RANS equations, some additional terms have been produced in the momentum (eq. 4) and energy conservation equation (eq. 5), named Reynolds stresses $\overline{\rho v_j' v_i'}$ and fluxes $\overline{\rho v_j' h'}$. These fluxes are modeled by the introduction of the turbulent viscosity η_t, which can be determined by applying appropriate turbulent models to complete the system of RANS equations. The system of conservation RANS equations regarding the issue presented was solved by applying the two-equation RNG k-ε turbulent model developed using Re-Normalization Group (RNG) methods [10]. The RNG k–ε turbulence model is robust, economic and reasonably accurate over a wide range of turbulent flow. This model solves transport equations for kinetic energy (k) and its dissipation rate (ε). It assumes that the flow is fully turbulent and the effects of molecular viscosity are negligible, and is valid only for fully turbulent flows.

The system of RANS equations, maintaining the mass, energy and momentum conservation equation, has

to be supplemented by the convection-diffusion equation (sometimes called transport equation) of mass species (ξ_n) of the reacting flow component n (eq. 6), which has, due to Reynolds averaging, an additional term called the turbulent mass species flux:

$$\frac{\partial}{\partial t}(\overline{\rho\xi_n}) + \frac{\partial}{\partial x_j}(\overline{\rho v_j \xi_n}) - \frac{\partial}{\partial x_j}\left[\left(\rho D_n + \frac{\eta_t}{Sc_t}\right)\frac{\partial \xi_n}{\partial x_j}\right] = \overline{I_{\xi_n}}$$

(6)

where Sc_t is turbulent Scmidt number and D_n is molecular diffusion coefficient of the component n.

The source terms of the energy ($\overline{I_T}$) and convection-diffusion equation ($\overline{I_{\xi_n}}$) are computed by the following two equations where $\overline{\omega_n}$ is computed by the turbulent combustion model:

$$\overline{I_T} = -\sum_{n=1}^{N}\Delta H_{f,n}^0\,\overline{\omega_n}$$

(7)

$$\overline{I_{\xi_n}} = M_n\overline{\omega_n}$$

(8)

where $\Delta H_{f,n}^0$ is the standard formation heat and M_n is the molecular mass of the component n. In the equations (eq. 7) and (eq. 8) the $\overline{\omega_n}$ stands for the formation or consumption rate of component n and is defined by:

$$\overline{\omega_n} = \frac{d\lfloor X_n \rfloor}{dt} = (V_n^{''} - V_n^{'})\overline{R_n}$$

(9)

which is written for the general form of the chemical reaction:

$$\sum_{n=1}^{N}V_n^{'}X_n \overset{k_f,k_b}{\Longleftrightarrow} \sum_{n=1}^{N}V_n^{''}X_n$$

(10)

where $V_n^{'}$ and $V_n^{''}$ are the stoichiometric coefficients of component for the reactants and products, respectively. The chemical reaction rate $\overline{R_n}$ in eq. (eq. 9) is calculated using appropriate combustion models.

In order to describe the oil droplet movement, the Lagrangian Particle Tracking Model was used, where it was necessary to consider that an oil droplet moves through a continuous component of the gas phase. Forces that act on every individual oil droplet, and influence its acceleration appear on account of the differences between the velocity of the oil droplet and the gas phase and also because of the gas phase displacement. We considered that every oil droplet is influenced by the buoyancy force F_B and the drag force F_D. Other forces, however, were not included, since the density of oil droplets is much larger than that of the gas phase:

$$m_p\frac{dv_p}{dt} = \underbrace{-\frac{1}{8}\pi\rho_f d^2 C_D|v_f - v_p|(v_f - v_p)}_{F_D} + \\ + \underbrace{\frac{1}{6}\pi d^3(\rho_p - \rho_f)g}_{F_B}$$

(11)

At sufficiently small value of particle Reynolds numbers (the viscous regime), fluid particles behave in the same manner as solid spherical particles. In this case the drag coefficient is well approximated by the Schiller-Neumann correlation which is defined as:

$$C_D = \frac{24}{Re}(1 + 0.15Re^{0.687})$$

(12)

At larger value of particle Reynolds numbers, the inertial or distorted particle regime and the surface tension effects become important. The fluid particles become, at first, nearly ellipsoidal in shape, and finally, spherical cap-shaped [11]. The drag coefficient of oil droplets was modeled using Ishii-Zuber Drag Model where the drag coefficient is approximately constant, independent of Reynolds number, but dependent on the particle shape through the dimensionless group known as the Eotvos number, which measures the ratio between gravitational and surface tension forces:

$$Eo = \frac{g \cdot \Delta\rho \cdot d_p^2}{\sigma}$$

(13)

where $\Delta\rho$ stands for the density difference between the phases, g is the gravitational acceleration and σ is the surface tension coefficient.

The Ishii-Zuber correlation is given as [12]:

$$C_D = \frac{2}{3}Eo^{\frac{1}{2}}$$

(14)

The liquid evaporation model is a model for particles with heat transfer and one component of mass transfer, and in which the continuous gas phase is at a higher temperature than the particles. The model uses two-mass transfer correlations depending on whether the droplet is above or below the boiling point. This is determined through the Antoine equation:

$$p_{sat} = p_{scale}\,exp^{\left(A - \frac{B}{T+C}\right)}$$

(15)

where p_{scale} is the pressure scale used to scale the units for the vapor pressure, A is the Antoine Reference State Constant, B is the Antoine Enthalpic Coefficient and C is the Antoine Temperature Coefficient.

The particle is boiling if the vapor pressure p_{sat} is greater than the gaseous pressure. When the particle is above the boiling point, the mass transfer is determined by the convective heat transfer:

$$\frac{dm}{dt} = -\frac{Q_C}{V}$$

(16)

When the particle is below the boiling point, the mass transfer is given by:

$$\frac{dm}{dt} = \pi \cdot d \cdot D \cdot Sh \cdot \frac{W_C}{W_G} \cdot \log\left(\frac{1-X}{1-X_G}\right) \qquad (17)$$

where W_C and W_G are the molecular weights of the vapor and the mixture in the continuous phase, while X and X_G are the molar fractions in the drop and gas phase. In either case, the rate of mass transfer is set to zero when all of the non-base substances in the particle evaporated.

The EDC model has been applied based on an assumption that chemical reactions are faster in comparison to diffusion processes. Besides, the numerical model uses the EDC model for the combustion of the volatile gases in the gas phase. The rate of progress of elementary reaction n in the EDC model is determined by the two following expressions for reactant (eq. 18) and product limiter (eq. 19):

$$\overline{R_n} = A\frac{\varepsilon}{k} min\left(\frac{[X_n]}{V_n^{''}}\right) \qquad (18)$$

where $[X_n]$ is the molar concentration of component n and including only the components of the reactants, A is a constant and its value varies from case to case (in our case $A = 4$).

$$\overline{R_n} = AB\frac{\varepsilon}{k}\left(\frac{\sum_{n=1}^{P}[X_n]M_n}{\sum_{n=1}^{P}V_n^{''}M_n}\right) \qquad (19)$$

where P includes all product components in the elementary reaction n (eq. 10) and B is additional model constant (in our case $B = -1$).

Because the radiation is also a physical important transport phenomena during the combustion the P1 radiation model has been chosen, since it proved as most appropriate [13-14]. The P1 radiation model is also a simplification of the Radiation Transport Equation which assumes that the radiation intensity is isotropic or direction independent at a given location in space.

3.2. Geometry of the Model

Before developing a numerical model, the geometry of the model (see fig. 2) has been created, including the combustion chamber in its original size, the oil burner torch together with the baffle plate for the combustion air supply, and the oil nozzle for the fuel supply. Special attention was paid to creating the oil burner torch, the baffle plate and the fuel supply, since the effect of the air flow swirling caused by the baffle plate of the oil burner has been considered. Specific details of the actual combustion chamber causing just a minor effect on the behaviors in the combustion chamber have been simplified and disregarded.

Great attention was given to mesh selection. It is important to adjust and adapt the required size of mesh control volumes according to the size of the oil nozzle and of the combustion chamber. In the expected flame front area, the mesh had to be appropriately discretized for sufficient inclusion of all complex special processes of the turbulent combustion. In the opposite case, the results would not have been precise enough, providing a distorted picture of actual behaviors. Selection of the mesh has a direct influence on a number of control volumes, while a higher number of control volumes prolongs the calculation time. From the aspect of calculation time, it is therefore reasonable to choose the number of volumes that is as small as possible and that still ensures qualitative results at appropriate calculation times. However, it is also necessary to consider the size and the form of the control volumes at critical spots that have to be appropriately discretized. It can easily happen that an inappropriate form and size of the mesh at these spots have an impact on the convergence of numerical results. Considering mentioned facts 705 881 control volumes have been applied.
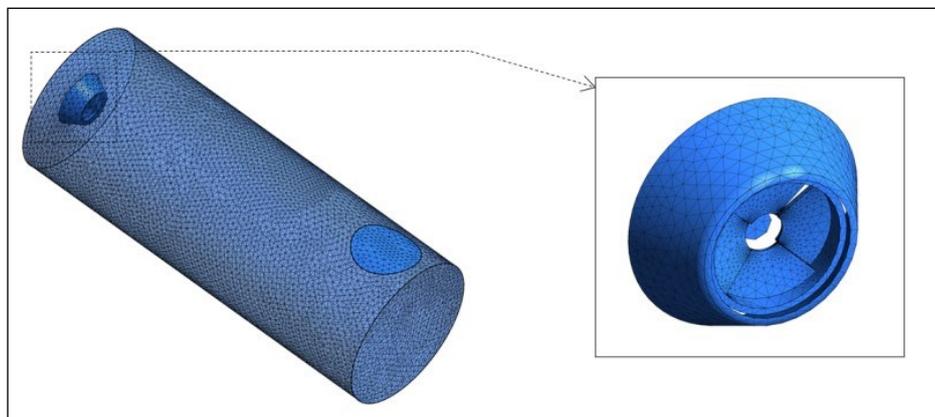
Figure 2. Discretized geometry and detailed view illustrating the blast tube and the torch of the oil burner.

3.3. Boundary Conditions

The calculation was based on the transient analysis with the time limit of 1 second, during which the periodical flow field should set up. In this study the High Resolution was used for the advection scheme which is more accurate than the Upwind Scheme [11] and First Order for turbulence because turbulence is a fairly diffusive process. The calculation of conservation equations was performed in time steps of 0.004 seconds. During each time step it was, however, necessary to specify eight additional non-linear iterations to ensure the conditions of complete convergence. In our case, the convergence criterion 10^{-4} was selected, which indicates that the calculation accuracy is satisfactory. In the calculation domain, two points were also selected, at which the velocity value was examined during the calculation. The velocity oscillation at these two points has stabilized after a certain time or, as the case may be, the oscillation has become periodical having the minimal amplitude. This indicates steady-state solution of the flow field at specific points.

Two-phase system of vaporization-combustion of the oil with air has been used. The required boundary conditions were determined at the following points: the INLET (mass flow of fuel, mass flow of air), the OUTLET (pressure), and the SURFACE OF THE BOILER JACKET (determined boundary condition on the wall – heat transfer (deducted heat flux), no-slip boundary condition – v=0, aggregation oil droplets on the wall). It is very difficult to determine the intensity of the turbulent movement of the air passing through the baffle plate into the combustion chamber. Therefore the medium intensity (5%) has been chosen. Specific boundary conditions, like the inlet mass flow of fuel, the mass flow rate of the air supply and the Sauter mean diameter of an oil droplet, had to be estimated and changed several times. Besides, the appropriate numerical models have been chosen to provide similar conditions under which the experiment was carried out, since not all volume measurements of quantities appearing during the combustion process and being possible to measure in the experiment were available. Some model parameters have been collected in tab. 1.

Table 1. Model parameters.

Air mass flow [kg/s]:	0.014952
Air temperature [K]:	297
Air mass fraction:	0.232 (O_2), 0.768 (N_2)
Turbulence Intensity:	Medium (5%)
Fuel mass flow [kg/s]:	0.000861
Fuel temperature [K]:	343
Liquid evaporation method:	Light oil modification
Coefficients of Antoine Equation:	A = 23.3, B = 5600 [K], C = 25 [K], p_{scale} = 1 [Pa]
Coefficient of EDC Combustion model:	A= 4, B = -1
Fluid Pair:	Gas Mixture‖Extra Light Fuel Oil
Heat Transfer Model:	Fluid dependent
Heat Transfer Model for Gas Mixture:	Thermal Energy
Heat Transfer Model for Extra Light Fuel Oil:	Particle Temperature
Particle Coupling:	Fully Coupled
InterPhase Heat Transfer:	Ranz Marshall
InterPhase Thermal Radiation Transfer:	Opaque
Buoyancy Model:	Full Buoyancy Model (Density Difference)
Buoyancy Turbulence:	Production and Dissipation
Wall temperature [K]:	363
Outlet Static Pressure [Pa]:	-3
Reference Pressure [atm]:	1

Actual distribution of oil droplets, which is the function of the diffusion oil nozzle and the diffusion parameters, was defined by applying the function of Rosin-Rammler distribution:

$$R = exp\left[-\left(\frac{d}{d_e}\right)^n\right]$$ (20)

with the diameter $d_e = 55\ \mu m$ and the spread parameter n, which is a measure of dispersion of particle sizes where lower values indicate wider dispersion, $n = 2.8$. The dispersion has been determined in the shape of a hollow cone with the angle 60° and the dispersion angle 5°, the injection velocity magnitude 28 m/s, and the injection oil droplet temperature 70 °C.

In fig. 3 it is demonstrated that the biggest oil droplets appear at the beginning of dispersion within the size range 100 μm. After that, oil droplets disperse into smaller ones and vaporize. As a result, conditions for dispersion fineness are fulfilled. Oil droplets of such size class represent conditions similar to those in the experiment. From combustion process modeling viewpoint, droplets should have various diameters that have different combustion times, since that is the only way to provide formation of a stable flame.
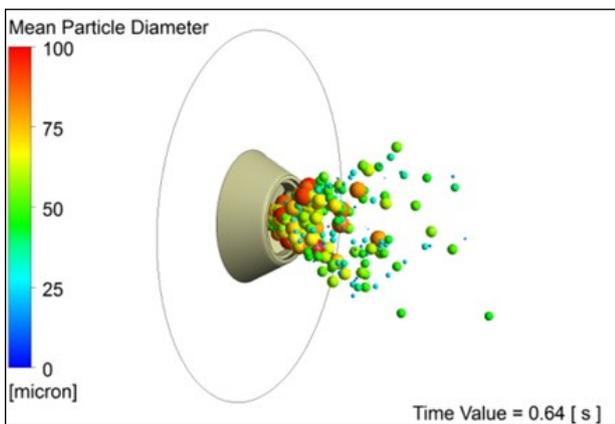
Figure 3. Distribution and size of oil droplets.

4. Results and Discussion

4.1. Numerical results

Flame is a typical feature of combustion, and includes a narrow area where basic physical-chemical processes of oxidation take place, and broadens through space filled with reactants. In most cases, flame can be visible, which is the consequence of the presence of different temperatures and molecules of intermediate combustion products.

High temperatures arise in the flame zone. This means that the temperature field in the highest

temperature range at the same time also presents the flame position (see fig. 4a). It is possible to conclude that in the flame front, high temperature gradients and changes in the reacting flow composition are present. The reacting flow is characterized by maximal combustion temperatures where their values depend on λ and the heat exchange rate with the environment. On the basis of the velocity field (see fig. 4b and 4c) it can be established that the highest velocities appear in the centre of the flame. This is understandable, since there is the greatest impact of the temperature gradients on the density, and consequently through the momentum equation also on the velocity components. The field of consumption of the air or O_2 concentrations is located within the combustion zone where fast consumption is typical (see fig. 4d). The excess of the O_2 mass concentration is distributed relatively equally outside the flame through the whole combustion chamber. After O_2 enters the combustion chamber, the concentration of H_2O (water vapor) (see fig. 4e) and of CO_2 (see fig. 4f) noticeably increases in the flame zone. An intensive chemical reaction of combustion namely takes place in the centre of the flame where the highest temperature is present. The concentration begins to distribute equally through the whole combustion chamber, what is also to be expected, since CO_2 as well as H_2O (water vapor) are products of complete combustion. The indicator of incomplete combustion is the presence of CO in combustion products (see fig. 4g) or in flue gases. The highest concentrations of CO appear immediately in front of the flame zone on the side of the fuel supply. Further, the combustion is complete, which indicates that there is enough air, and that conditions for complete combustion are ensured.

4a) Temperature flame field

4b) Velocity field

4c) Velocity field (vectors)

4d) Air concentration field (O_2)

4e) H_2O concentration field

4f) CO_2 concentration field

4g) CO concentration field

4h) NO concentration field

4i) N_2 concentration field

4j) Temperature load of the combustion device wall

4k) Streamlines through the combustion chamber (2D)

4l) Streamlines through the combustion chamber (3D)

Figure 4. Numerical results.

Thermal NO represents 95% of all NO_X, which arise through the combustion of ELFO (see fig. 4h). The highest concentrations of NO appear in the flame area where the highest temperatures and enough O_2 for oxidation of N_2 are present. The reasons for formation of thermal NO are in particular high temperatures near the flame front. For their appearance sufficient quantity of O_2 is needed. O_2 reacts then with N_2 (see fig. 4i), which leads to creation of thermal NO. The temperature load of the combustion device wall (see fig. 4j) shows that the back wall is most exposed to the temperature on account of the changeable length of the flame. 2D surface streamlines (see fig. 4k) and 3D streamlines (see fig. 4l) shows exact information about behaviors within the combustion chamber. The findings in our case indicate that the flow is extremely turbulent and completely unsteady. The numerical results confirm that an appropriate λ_{opt} was determined in the scope of the experiment, and consequently the conditions for complete combustion were ensured.

4.2. CFD Validation with Experimental Data

Numerical results had to be properly verified in order to obtain information about the suitability of the numerical model. The comparison between different results is in Table 2: numerical results, results of experimental measurements, analytical calculation results based on solving the empirical stoichiometric equations for liquid fuels, and results taken from literature. Comparison in tab. 2 shows that these results are in good agreement with each other (deviation is less than 5%).

In the scope of the experiment has been possible to record the appearance of the turbulent flame, and then compare it with the CFD numerical model. The findings indicate that the area with the highest temperatures is present in the flame center where the injection of the liquid fuel is also performed (see fig. 5).

Deviations between numerical and experimental results appear because the numerical analysis does not consider the effect of atomization of liquid fuel into oil droplets. In carrying out the experiment, however, the following factors should be taken into account: permanent air pressure changes, permanent air temperature changes, permanent pressure changes in the furnace, and other weighting factors. Despite these simplifications, the numerical model provides sufficiently accurate description of the combustion physical behavior.

Table 2. Comparison of results.

$\lambda = 1,2$	Numerical [vol. %]	Experimental [vol. %]	Analytical [vol. %]	Literature [15] [vol. %]	Literature [16] [vol. %]
$O_{2,wet}$	3.22	3.16	3.32	3.4	3.28
$O_{2,dry}$	3.61	3.5	3.71	3.77	3.69
$CO_{2,dry}$	12.72	12.8	12.62	12.6	12.74

5a) Actual appearance of the turbulent flow in the observation period

5b) CFD appearance of the turbulent flow according to the numerical model
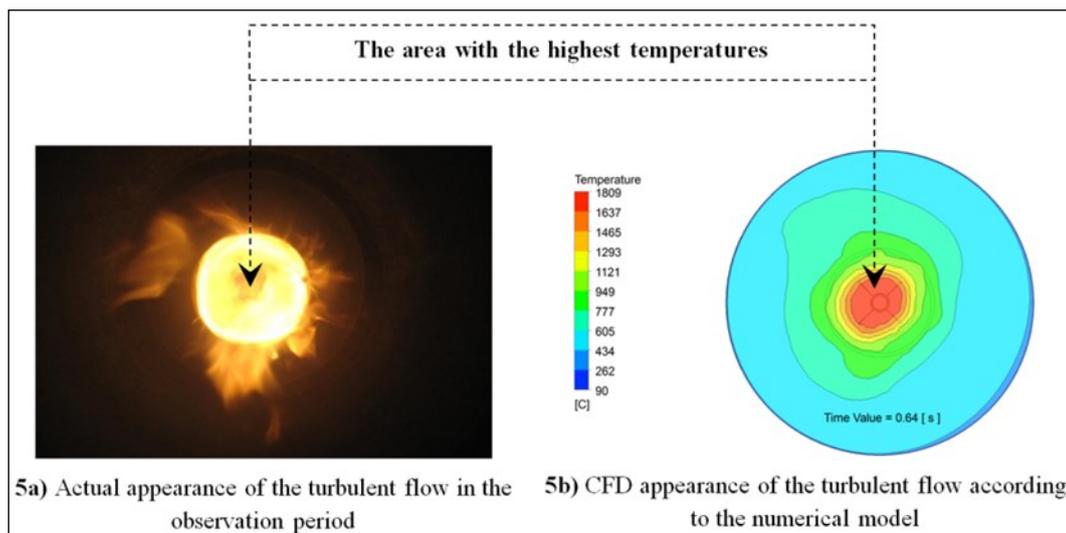
Figure 5. Comparison of the turbulent flame in the experiment and in the CFD analysis.

5. Conclusion

To sum up, the paper illustrates that our description of the turbulent combustion process of liquid fuels and physical behaviors inside the combustion chamber is sufficiently accurate. This description is namely based on the selected numerical models in the scope of the CFD as well as on assumptions and experimental presuppositions. The findings were confirmed with the presented case of ELFO combustion in a small combustion device. In practice oil burner always need to operate with some excess of air (generally 15-20% of the required stoichiometric amount) to achieve a complete combustion. The suggested optimal air-fuel ratio for the presented case is $\lambda_{opt} = 1.2$, which is based on detailed analysis of the experimental measurement results of flue gas emissions. The most sensitive indicator of the incomplete combustion is concentration of CO, which is formed because of insufficient amount of the oxygen. Another reason for the incomplete combustion can also be an improper mixing of the combustion air with the fuel. Therefore the CO can be regarded as a good indicator of the combustion quality. Incomplete combustion means that less energy is released and combustion efficiency is reduced. Appropriate settings of the oil burner can enable fuel savings up to 10%, sometimes even more. That is why combustion control and determination of an appropriate optimal air-fuel ratio λ_{opt} are of great importance. By applying the appropriate λ_{opt}, it can be established, whether the optimal combustion is achieved, since only 1% of CO in flue gases would be enough to cause an increase of the furnace losses of 4 to 5%.

Literature

1. J. Broukal, J. Hajek, Wall Heat Fluxes in Swirling Combustion of Extra Light Fuel Oil in Large Scale Test Combustor: Experiment and Modelling Using Eddy Dissipation Model. 13th Conference on Process Integration, Modelling and Optimisation for Energy Saving and Pollution Reduction, Book Series: Chemical Engineering Transactions, Volume 21, 1111--1116, 2010.

2. FK Jager, H. Kohne, CFD modelling in process burner development: Combustion of light residual fuel oils. Computational Fluid and Solid Mechanics, Vols 1 and 2, Proceedings, 966--970, 2003.

3. A. Saario, A. Rebola, PJ Coelho, M. Costa, A. Oksanen, Heavy fuel oil combustion in a cylindrical laboratory furnace: measurements and modeling. Fuel, Volume 84, 359--369, 2005.

4. DR Schneider, Z. Bogdan, Modelling of SO3 formation in the flame of a heavy-oil fired furnace.

Chemical and Biological Engineering Quarterly, Volume 17, 175--181, 2003.

5. M. Takei, R. Weber, T. Niioka, Mathematical modeling of industrial furnaces considering detailed oil spray characteristics. Combustion Science and Technology, Volume 175, 1237--1262, 2003.

6. T. Poinsot, D. Veynante, Theoretical and Numerical Combustion, Second Edition, 2005.

7. C. K. Westbrok, F. L. Dryer, Simplified Reaction Mechanisms for the Oxidation of Hydrocarbon Fuels in Flames. Combustion Science and Technology, 31--43, 1981.

8. N. Peters, Turbulent combustion, Cambridge, 2004.

9. J. Warnatz, U. Maas, R.W. Dibble, Combustion: Physical and Chemical Fundamentals, Modelling and Simulation, Experiments, Pollutant Formation, Springer Verlag, Berlin Heidelberg, 1996.

10. Yakhot, V., Orszag, S.A., Thangam, S., Gatski, T.B. & Speziale, C.G., Development of turbulence models for shear flows by a double expansion technique. Physics of Fluids A, Vol. 4, No. 7, pp1510-1520, 1992.

11. Ansys, Ansys – CFX Documentation, Release 13, November 2010.

12. Ishii M. and Zuber N., Drag coefficient and relative velocity in bubbly, droplet or particulate flows. AIChE Journal, Volume25, Issue 5, 843--855, 1979.

13. A. Habibi, B. Merci, G. J. Heynderickx, Impact of radiation models in CFD simulations of steam cracking furnaces. Computer & Chemical Engineering, 1389--1406, Volume 31, Issue 11, 2007.

14. B. Rajh, Experimental – numerical analysis of oil combustion in a small burning device, diploma work, Maribor, 2009.

15. Weishaupt, Technische Arbeitsblätter, 2001.

16. J. Oman, A. Senegačnik, A. Mirandola: Air, fuels and flue gases: physical properties and combustion constants. Padova: Progetto, 106--109, 2006.